Coherent Raman scanning fiber endoscopy

Brian G. Saar,[1,4] Richard S. Johnston,[2] Christian W. Freudiger,[1,3] X. Sunney Xie,[1,5] and Eric J. Seibel[2,6]

[1]*Department of Chemistry and Chemical Biology, Harvard University, Cambridge, Massachusetts 02138, USA*

[2]*Human Photonics Laboratory, University of Washington, Seattle, Washington 98195, USA*

[3]*Department of Physics, Harvard University, Cambridge, Massachusetts 02138, USA*

[4]*Present address: MIT Lincoln Laboratory, Lexington, Massachusetts 02420, USA*

[5]*e-mail: xie@chemistry.harvard.edu*

[6]*e-mail: eseibel@u.washington.edu*

Received March 28, 2011; revised May 7, 2011; accepted May 13, 2011;
posted May 13, 2011 (Doc. ID 144659); published June 20, 2011

Coherent Raman scattering methods allow for label-free imaging of tissue with chemical contrast and high spatial and temporal resolution. However, their imaging depth in scattering tissue is limited to less than 1 mm, requiring the development of endoscopes to obtain images deep inside the body. Here, we describe a coherent Raman endoscope that provides stimulated Raman scattering images at seven frames per second using a miniaturized fiber scanner, a custom-designed objective lens, and an optimized scheme for collection of scattered light from the tissue. We characterize the system and demonstrate chemical selectivity in mouse tissue images.

OCIS codes: 170.2150, 190.4180, 290.5910.

Optical imaging methods are vital in medical diagnostics because they offer high spatial resolution and excellent contrast at high acquisition speeds compared to widely used radiological imaging techniques such as magnetic resonance imaging, position emission tomography, or x-ray computed tomography. Optical disease diagnosis can be enhanced in sensitivity by the application of exogenous labels to obtain molecularly specific information from the tissue, but these are sometimes toxic. In addition, most biological tissues exhibit strong absorption and scattering of light, so the penetration of high-resolution optical methods is limited to a few millimeters, restricting optical diagnostics.

Endoscopy circumvents the penetration depth limit by bringing an optical system into proximity with tissues of interest, even inside a living patient. Optical endoscopes with white light contrast have revolutionized surgery, allowing minimally invasive procedures to be performed inside the body [1]. Advanced endoscopic contrast modes have been reported for wide-field fluorescence and narrowband imaging [2,3], confocal reflectance [4] and fluorescence [5], and two-photon fluorescence [3,6–8].

The combination of novel label-free optical imaging modalities with endoscopic devices presents new opportunities for *in situ* diagnostics. Coherent Raman scattering (CRS) [9–11] methods offer label-free chemical contrast with microscopic resolution and have the potential to provide *in situ* virtual pathology on fresh tissue without the excision, fixation, slicing, and staining procedure required by traditional histopathology [12,13]. However, coherent Raman methods have required laser scanning microscopes. Such systems can be miniaturized [14], but the use of optical fiber delivery is highly desirable for flexibility in clinical applications. Several groups have reported optical modeling [15] and progress toward realizing optical-fiber-delivered CRS imaging systems, but required either sample scanning [16] or scanning mirrors [17] and long scan times. Here, we report a miniaturized coherent Raman imaging system based on a compact scanning fiber endoscope (SFE) [18], a step toward translating coherent Raman imaging methods into clinical practice. In CRS, which refers to both coherent anti-Stokes Raman scattering (CARS) [9,10] and stimulated Raman scattering (SRS) [11,19–22], laser beams at two frequencies, called the pump, ω_p, and Stokes, ω_S, frequencies, are used to illuminate the sample. When the difference frequency between the two beams is tuned to match an intrinsic molecular vibrational frequency in the sample, ω_{vib}, several nonlinear interactions occur. New light is generated at the anti-Stokes frequency, $\omega_{\mathrm{as}} = 2\omega_p - \omega_S$, by the CARS process, and some intensity is transferred from the pump to the Stokes beam by the SRS process [Fig. 1(a)]. Both processes offer chemical selectivity, high spatial resolution, and video-rate imaging speeds *in vivo* in living animals [23] and humans [22]. SRS offers more desirable contrast that depends linearly on the target species concentration and is free from the image artifacts and nonresonant background that plague CARS imaging [11], but has thus far not been implemented in an endoscope or miniature microscope format.

Because SRS imaging involves measurement of small intensity changes in the pump beam, we make use of a highly sensitive modulation transfer scheme in which we amplitude modulate the Stokes beam at a high reference frequency (e.g., 10 MHz), illuminate the sample with both the pump and Stokes beams, and then detect only the pump beam with a photodiode (PD) behind an optical filter (OF) that blocks the Stokes beam. The PD signal is demodulated by a lock-in amplifier (LIA) tuned to the reference frequency that only detects amplitude modulation when SRS occurs in the sample [11].

Images are formed by scanning the laser over the sample and recording the modulation of the pump beam as a function of position. In this Letter, the laser system that excites the sample is similar to one described recently [22]. It is based on a passively mode-locked Nd:YVO_4 laser (picoTrain, high Q laser), which provides 7 ps pulses at a repetition rate of 80 MHz. A portion of the output at 1064 nm is the Stokes beam for the CRS processes, and the remainder of the output is frequency doubled and used to synchronously pump an optical parametric

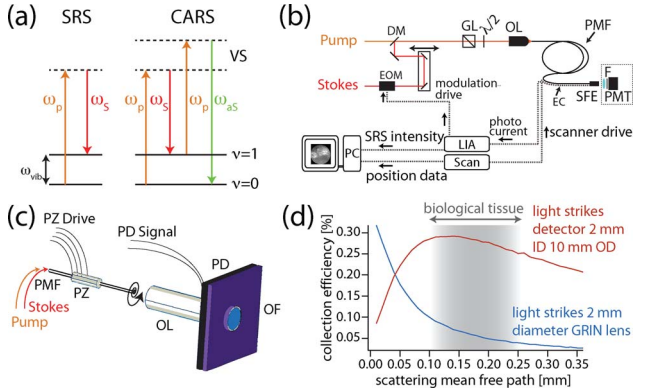

Fig. 1. (a) Energy diagrams of the SRS and CARS processes. (b) Schematic of the device: the Stokes laser beam is amplitude modulated using an EOM driven by a 10 MHz waveform, temporally delayed, and combined with the pump beam on a DM. The beams pass through a Glan-Laser (GL) prism, and their polarization is rotated by a $\lambda/2$ plate to match the PM axis of a 1 m PM fiber (PMF). Light is coupled into the fiber through an OL (10× 0.4 NA Olympus). The distal tip of the fiber is moved using a SFE. The scan is driven by control electronics through electrical cables, which also report the scanner position to a personal computer to record images. The photocurrent from the detector in the SFE is demodulated using an LIA, which also provides the reference frequency to the EOM. The demodulated signal is the image intensity. For transmitted CARS detection, the SFE tip is positioned in front of a photomultiplier tube detector with an OF (labeled F) that transmits only the anti-Stokes wavelength. (c) Detailed view of the SFE. The single-mode PMF passes through a PZ tube patterned with four electrodes, which are actuated by the scan controller. The light from the PMF is relayed to the sample by a GRIN objective lens (OL) and collected by a PD after filtering by an OF. (d) Simulations show that, for tissue with scattering mean free path of 0.1–0.25 mm, forward-traveling SRS light is not efficiently collected by the objective lens. Collection by a PD surrounding the detector can achieve >30% efficiency of the light that propagates from the focus.

oscillator (OPO; Levante Emerald, APE GmbH), which generates a tunable pump beam near 800 nm.

The Stokes beam is modulated by an electro-optic modulator (EOM; Raicol Crystals, Ltd.) at 10 MHz and combined in space on a dichroic mirror (DM; 1064dcrb, Chroma Technology) with the OPO output. The two beams are linearly polarized and, after passing through an achromatic wave plate (AHWP05M-980, Thorlabs), they are coupled into a single-mode polarization-maintaining (PM) optical fiber (PM780-HP, Thorlabs).

The optical fiber delivers the laser beams to the sample [Fig. 1(b)], and the image is scanned using a miniature piezo-electric (PZ) actuator to drive the fiber tip at its mechanical resonance frequency in an expanding spiral [Fig. 1(c)]. A scan rate of seven frames per second can be achieved. The scan pattern is actuated by passing the optical fiber through a small (<0.5 mm diameter) piezo-electrically active ceramic tube that is radially patterned with four electrodes. To achieve the spiral scan, one pair of opposing electrodes is driven with a sine wave and the other is driven with a cosine wave, both with linearly expanding envelope functions. The scan driver electronics track the fiber tip for image reconstruction. This SFE provides a unique combination of small package size, high frame rate, and adaptability to a variety of laser scanning techniques.

The laser light from the fiber output is focused onto the sample by a gradient index (GRIN) objective lens (OL). Single element GRIN lenses have large axial chromatic aberrations, which significantly degrade the nonlinear signal-generation efficiency. For this reason, we utilized an OL consisting of two GRIN elements sandwiching a diffractive optic, which was designed to have zero axial chromatic aberration at the chosen wavelengths, an NA of 0.3, a free working distance of 150 μm, and an outer diameter of 1.4 mm. Typical power levels of ~130 mW are used, which is similar to those previously used for *in vivo* imaging [23].

For light collection, we observed that the modulated pump beam that travels forward from the focus is redirected back toward the tissue surface by multiple scattering within turbid tissue. Nonsequential ray-tracing simulations [Fig. 1(d) and [22]] show that using a large area PD surrounding the excitation lens allows for optimal collection efficiency. In this study, we utilized a 10 mm × 10 mm PD, but simulations indicate that a 5 mm diameter circular PD would achieve ~75% of the present collection efficiency. Thus, we surrounded the lens with a back-biased silicon PIN PD (FDS1010, Thorlabs) through which we drilled a 2 mm diameter hole for the OL [Fig. 1(c)]. A custom-designed OF identical to one in a previous report [22] blocked the modulated Stokes beam from reaching the PD. As observed previously [16], because picosecond pulses are employed in CRS, ordinary silica fibers can be used for light delivery over a length of 1 m without self-phase modulation broadening the optical spectrum [Fig. 2(a)] beyond the intrinsic Raman linewidth (~1 nm at 800 nm).

We verified the spatial resolution of the system with transmission mode CARS images of 2 μm diameter beads [Fig. 2(b)]. Bead sizes of 1.3 μm (FWHM) demonstrate the ability to clearly resolve 2 μm objects across the 80 μm diameter field of view. By axially translating the beads in 1 μm steps, we measured the axial FWHM of 6.5 μm.

We then tested the ability of the system to obtain SRS images in mouse skin tissue at seven frames per second (with a 500 pixel diameter field of view). This required the use of a custom LIA [22] to process the SRS signal.

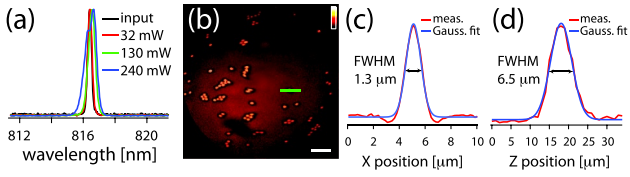

Fig. 2. (a) Optical spectrum of the pump laser beam at the fiber input (black) and propagating through 1 m of PMF with the indicated power level at the fiber output. Even with 240 mW of power output, the FWHM is 0.85 nm, indicating that we can still resolve individual Raman bands with intrinsic linewidths of around ~1 nm. (b) CARS image of 2 μm polystyrene beads coated on a glass slide. Individual beads can be easily resolved, indicating a lateral resolution better than 2 μm. Scale, 10 μm. (c) Measured lateral profile (red) and Gaussian fit (blue) of an individual 2 μm bead, indicating the lateral FWHM of 1.3 μm for the bead indicated in green in (b). (d) Axial profile of an individual 2 μm bead, indicating an axial FWHM of 6.5 μm and demonstrating optical sectioning capability.

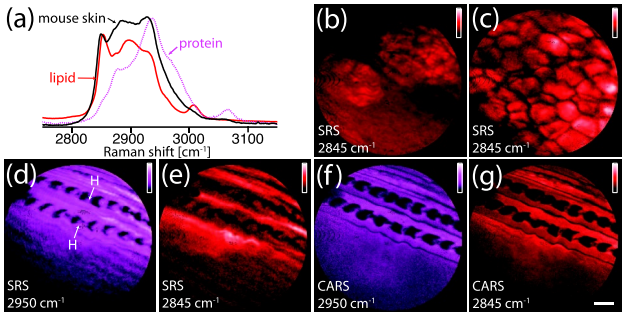

Fig. 3. CRS images with the endoscope. (a) Raman spectra of mouse skin (black), a representative lipid compound (oleic acid, red), and a representative protein compound (soy protein extract, dotted magenta). (b) SRS image of a sebaceous gland approximately 30 μm deep in mouse skin. (c) SRS image of the subcutaneous fat approximately 50 μm deep in mouse skin, acquired at seven frames per second in the epi direction. (d), (e) SRS images of hairs near the surface of a mouse skin with protein (d) and lipid (e) contrast. Hair is rich in protein and coated in lipids, as indicated by the SRS images. (f), (g) CARS images obtained simultaneously with (d) and (e) in the transmitted direction, showing a lack of CARS contrast for protein (f) and lipid (g). Field of view, 80 μm; scale, 10 μm.

With this system, we could tune into the CH_2 stretching vibration of lipids [Fig. 3(a)] to record an image of the sebaceous gland [Fig. 3(b)] and subcutaneous fat in mouse skin at a depth of ~50 μm [Fig. 3(c)]. Image contrast disappeared and the signal level dropped to the demodulator noise floor when the OL was not focused in the tissue sample, indicating a negligible background from nonlinear effects within the fiber.

We tested the chemical selectivity of the system by recording images of mouse hair near the surface of the tissue. Hair is known to be rich in protein and coated with a layer of lipids that are secreted by the mouse skin. By tuning the laser system to match the CH_3 stretching resonance at 2950 cm^{-1} [Figs. 3(d) and 3(f)] or the CH_2 stretching resonance at 2845 cm^{-1} [Figs. 3(e) and 3(g)], we could see in the SRS images either the protein-rich center of the hair [Fig. 3(d) indicated by the "*H*" labels) or the lipid-rich coating of the hair [Fig. 3(e)]. This tuning was previously observed in a bulk SRS microscope [22] and demonstrates that the chemical contrast in tissue matches the behavior of the Raman spectrum [Fig. 3(a)].

However, simultaneous forward CARS detection [Figs. 3(f) and 3(g)] did not manifest this behavior because the nonresonant background of CARS limits the chemical selectivity of the technique and does not allow clear discrimination between lipids and proteins based on CH_2 and CH_3 stretching images. This demonstrates the importance of obtaining SRS contrast because recent work utilizing this contrast has shown that SRS has pathology-like diagnostic capability in fresh tissue [13].

In summary, the system described here demonstrates that the technical challenges for CRS endoscopy, fiber delivery, laser scanning, focusing, light collection, and demodulation can be solved. Improvements to the device, particularly the use of fiber lasers, will increase ease of use, facilitating clinical translation of CRS.

We thank C. Lee and D. Melville for design and fabrication of the SFE at the University of Washington; B. Messerschmidt of GrinTech GmbH for design and fabrication of the GRIN lens; and M. Roeffaers, G. Holtom, D. Fu, and X. Zhang for helpful discussions. C. W. Freudiger acknowledges support from a Boehringer Ingelheim Fonds Ph.D. scholarship. This work was supported by National Institutes of Health (NIH) grants to E. J. Seibel (R33 CA 094303 and R21 EB012666) and a T-R01 grant (1R01EB010244-01) to X. S. Xie, the University of Washington Mechanical Engineering Royalty Fund, and the Harvard University Office of Technology Development Accelerator Fund.

References

1. M. J. Mack, J. Am. Med. Assoc. **285**, 568 (2001).
2. K. Gono, IEEE J. Quantum Electron. **14**, 62 (2008).
3. C. M. Lee, C. J. Engelbrecht, T. D. Soper, F. Helmchen, and E. J. Seibel, J. Biophoton. **3**, 385 (2010).
4. C. Boudoux, S. Yun, W. Oh, W. White, N. Iftimia, M. Shishkov, B. Bouma, and G. Tearney, Opt. Express **13**, 8214 (2005).
5. R. Kiesslich, J. Burg, M. Vieth, J. Gnaendiger, M. Enders, P. Delaney, A. Polglase, W. McLaren, D. Janell, and S. Thomas, Gastroenterology **127**, 706 (2004).
6. M. E. Llewellyn, R. P. J. Barretto, S. L. Delp, and M. J. Schnitzer, Nature **454**, 784 (2008).
7. C. L. Hoy, N. J. Durr, P. Chen, W. Piyawattanametha, H. Ra, O. Solgaard, and A. Ben-Yakar, Opt. Express **16**, 9996 (2008).
8. P. Kim, M. Puoris'haag, D. Côté, C. P. Lin, and S. H. Yun, J. Biomed. Opt. **13**, 010501 (2008).
9. A. Zumbusch, G. R. Holtom, and X. S. Xie, Phys. Rev. Lett. **82**, 4142 (1999).
10. C. L. Evans and X. S. Xie, Annu. Rev. Anal. Chem. **1**, 883 (2008).
11. C. W. Freudiger, W. Min, B. G. Saar, S. Lu, G. R. Holtom, C. He, J. C. Tsai, J. X. Kang, and X. S. Xie, Science **322**, 1857 (2008).
12. C. L. Evans, X. Xu, S. Kesari, X. S. Xie, S. T. C. Wong, and G. S. Young, Opt. Express **15**, 12076 (2007).
13. C. W. Freudiger, B. G. Saar, D. A. Orringer, R. Pfannl, Q. Zeng, L. Ottoboni, T. Chen, W. Ying, R. D. Folkerth, C. A. French, W. R. Welch, C. Waeber, J. R. Sims, P. L. De Jager, O. Sagher, M. A. Philbert, X. Xu, S. Kesari, X. S. Xie, and G. S. Young, "Stain-free histopathology with stimulated Raman scattering microscopy," submitted to Proc. Natl. Acad. Sci. USA.
14. S. Murugkar, B. Smith, P. Srivastava, A. Moica, M. Naji, C. Brideau, P. K. Stys, and H. Anis, Opt. Express **18**, 23796 (2010).
15. I. Veilleux, M. Doucet, P. Coté, S. Verreault, M. Fortin, P. Paradis, S. Leclair, R. S. Da Costa, B. C. Wilson, and E. J. Seibel, Proc. SPIE **7558**, 75580D (2010).
16. F. Légaré, C. L. Evans, F. Ganikhanov, and X. S. Xie, Opt. Express **14**, 4427 (2006).
17. M. Balu, G. Liu, Z. Chen, B. J. Tromberg, and E. O. Potma, Opt. Express **18**, 2380 (2010).
18. E. J. Seibel, C. M. Brown, J. A. Dominitz, and M. B. Kimmey, Gastrointest. Endosc. Clin. N. Am. **18**, 467 (2008).
19. E. Ploetz, S. Laimgruber, S. Berner, W. Zinth, and P. Gilch, Appl. Phys. B **87**, 389 (2007).
20. Y. Ozeki, F. Dake, S. Kajiyama, K. Fukui, and K. Itoh, Opt. Express **17**, 3651 (2009).
21. P. Nandakumar, A. Kovalev, and A. Volkmer, New J. Phys. **11**, 033026 (2009).
22. B. G. Saar, C. W. Freudiger, J. Reichman, C. M. Stanley, G. R. Holtom, and X. S. Xie, Science **330**, 1368 (2010).
23. C. L. Evans, E. O. Potma, M. Puoris'haag, D. Côté, C. P. Lin, and X. S. Xie, Proc. Natl. Acad. Sci. USA **102**, 16807 (2005).